Materials Express

Copyright © 2012 by American Scientific Publishers
All rights reserved.
Printed in the United States of America

2158-5849/2012/2/265/010
doi:10.1166/mex.2012.1083
www.aspbs.com/mex

Fluorescent Superparamagnetic Iron Oxide Core–Shell Nanoprobes for Multimodal Cellular Imaging

Sasidharan Smitha[1,*], Vadakkenchery S. Haseena[1], Tharangattu N. Narayanan[2], Antony P. Reena Mary[1], Pulickel M. Ajayan[2], Jayesh Puthumana[3], Anas A. Aziz[4], Rebeca R. Aburto[2,5], Sendurai A. Mani[5], Pattayil A. Joy[6], and Maliemadom R. Anantharaman[1]

[1]*Department of Physics, Cochin University of Science and Technology, Cochin, Kerala 682022, India*
[2]*Department of Mechanical Engineering and Materials Science, Rice University, Texas, TX 77005, USA*
[3]*National Centre for Aquatic Animal Health, Cochin University of Science and Technology, Kerala 682016, India*
[4]*National Institute of Oceanography (CSIR), Cochin, Kerala 682018, India*
[5]*Department of Molecular Pathology, MD Anderson Cancer Center Houston, Texas, TX 77030, USA*
[6]*Physical Chemistry Division, National Chemical Laboratory, Pune 411008, India*

Delivered by Publishing Technology to: Cochin University of Science and Technology
IP: 14.139.185.18 On: Fri, 01 Jun 2012 05:40:08
Copyright: American Scientific Publishers

Multimodal imaging agents that combine magnetic and fluorescent imaging capabilities are desirable for the high spatial and temporal resolution. In the present work, we report the synthesis of multifunctional fluorescent ferrofluids using iron oxide as the magnetic core and rhodamine B as fluorochrome shell. The core–shell structure was designed in such a way that fluorescence quenching due to the inner magnetic core was minimized by an intermediate layer of silica. The intermediate passive layer of silica was realized by a novel method which involves the esterification reaction between the epoxy group of prehydrolysed 3-Glyidoxypropyltrimethoxysilane and the surfactant over iron oxide. The as-synthesized ferrofluids have a high saturation magnetization in the range of 62–65 emu/g and were found to emit light of wavelength 640 nm ($\lambda_{excitation} = 446$ nm). Time resolved life time decay analysis showed a bi-exponential decay pattern with an increase in the decay life time in the presence of intermediate silica layer. Cytotoxicity studies confirmed the cell viability of these materials. The *in vitro* MRI imaging illustrated a high contrast when these multimodal nano probes were employed and the R2 relaxivity of these sample was found to be 334 $mM^{-1}s^{-1}$ which reveals its high potential as a T2 contrast enhancing agent.

Keywords: SPION, GPTMS, Multimodal Imaging, MRI Imaging, T2 Contrast Agent.

1. INTRODUCTION

Superparamagnetic iron oxide nanoparticles (SPIONs) owing to its finite size and fast response to applied magnetic fields with negligible remanence and coercivity, has gained significance as a potential candidate for various scientific and technological applications such as magnetic storage media, contrast enhancing agents for magnetic resonance imaging (MRI), cell labeling, cell tracking, cytometry, magnetic separation and targeted drug delivery devices.[1–4] The cellular imaging has become an inevitable diagnosis methodology for the effective treatment of various diseases in the modern world of medicine.[5–6] The computed tomography (CT), nuclear imaging (positron emission tomography, single photon emission computed tomography), optical and magnetic resonance imaging (MRI) have made profound contributions in the diagnosis and therapy.[7–9] However each imaging modality has its own advantages and limitations as far as sensitivity and resolution is concerned.[7] Even though MRI has excellent soft tissue contrast, it has a very low sensitivity whereas the major draw backs of optical imaging are poor depth

*Author to whom correspondence should be addressed.
Email: smissmis@gmail.com

Article

penetration and low absolute quantitative accuracy due to the absorption of light in tissues.[10] Therefore researchers are trying to integrate different imaging modalities synergistically to facilitate efficient diagnosis and therapy.[8–14] The combination of MRI and optical imaging will facilitate the high spatial and temporal resolution of optical imaging and depth of magnetic imaging.[10, 14] Due to the unique physical properties of SPIONs, it has long been studied as a contrast enhancing agent in MRI.[15] The incorporation of fluorescent materials in to these SPIONs can provide a new multimodal imaging platform which opens up new avenues for the diagnosis and therapy encompassing photodynamic and hyperthermic abilities also.[12] These multimodal materials could be easily controlled by an external magnetic field and can be monitored by MRI and fluorescent microscopy. They can also act as nano-blocks to fabricate various nanoelectronic and photonic devices in which the magnetic nanoparticles can be controlled by an external magnetic field and their positioning can be visualized using fluorescence confocal microscopy.[12]

Even though these fluorescent magnetic materials have tremendous application in biomedical fields, this research field still remains in infancy due to the complexities in the synthesis procedures.[12, 16–19] The major challenges in the synthesis of magnetic-fluorescent materials are the quenching of the fluorescence of the particle by the magnetic core due to the energy/charge transfer between metal ions and chromophore, and the agglomeration of particles during the multi-step preparation stages.[10] The quenching could be minimized by providing an intermediate shell between the magnetic core and the outer layer of fluorescent molecules.[19] Therefore many synthesis strategies include core–shell nanostructures in which intermediate shells consists of polymers, surfactants or silica.[10] The advantages of silica coating is its inertness, optical transparency, ease of functionalisation, biocompatibility and stability in most of the biosystems.[19–22] Sol–gel coatings using tetraethoxysilanes and 3-aminopropyltrimethoxysilane has been reported to synthesize the core–shell nanostructures of magnetic fluorescent materials.[12, 23] However the use of silanes that possess versatile groups such as epoxy will be more advantageous for the surface modification of magnetic nanoparticles since it can act as a linker between magnetic nanoparticles and additional functionalizing agents such as antibodies, proteins, dyes, drugs etc. Even though 3-glycidoxypropyltrimethoxysilane (GPTMS) has been widely used for the synthesis of organic-inorganic hybrid materials due to its flexible epoxy and alkoxy groups, a few reports are available for its application for the surface engineering of magnetic nanoparticles.[24, 25] Quantum dots of heavy metal ions or organic dyes are the frequently used fluorophores for the synthesis of magnetic fluorescent materials. However quantum dots incorporated fluorescent materials are not recommended for biomedical applications due to its toxicity and easy sustainability to surrounding environments which will affect the fluorescence.[26–28] Rhodamine B has been proved as a nontoxic fluorescent molecule that can be used for *in vitro* and *in vivo* applications.[10, 18, 20] Therefore the present work has emphasis on the synthesis of fluorescent ferrofluids through a novel method by conjugating rhodamine dye molecules on to the magnetic nanoparticles employing a passive coating of silica using GPTMS. Prior to conjugation with dye, the iron oxide particles were treated with a prehydrolysed GPTMS so as to avoid fluorescence quenching. Structural, optical and magnetic characterizations of the samples were carried out using Fourier transform infrared spectrophotometer (FT-IR), ultraviolet-visible spectrophotometer (UV), photoluminescence spectrophotometer (PL), X-ray diffraction technique (XRD), transmission electron microscope, vibrational sample magnetometry (VSM) and zeta potential measurements. The cytotoxicity was evaluated on human L312 embryonic lung cells following XTT (2, 3-bis[2-methoxy-4-nitro-5-sulfopheny]-2H-tetrazolium-5-carboxyanilide inner salt) assay.

2. EXPERIMENTAL DETAILS

2.1. Chemicals

Ferrous sulphate, ferric chloride, ammonia, isopropanol, citric acid and rhodamine B were purchased from Merck, India Ltd. GPTMS was from Aldrich Chemicals. All the chemicals used were of analytical grade and used without further purification.

2.2. Synthesis of Ferrofluids

SPIONS were prepared by the standard co-precipitation method using $FeSO_4$ and $FeCl_3$ as precursors in 1:2 molar ratio.[29, 30] A homogenous solution of $FeSO_4$ and $FeCl_3$ in water medium was mixed under stirring in a magnetic stirrer. Ammonium hydroxide was added to this reaction mixture till the pH reaches ~10. The stirring was continued for half an hour. The reddish brown precipitate formed was heated at 80 °C to expel excess ammonia. Further the solution was separated using electromagnet of 1 T and washed four times using distilled water. About 20 ml of distilled water is added to the washed precipitate. Further about 1 g citric acid dissolved in 10 ml distilled water was added to the above solution and kept for stirring for about one hour. Finally the solution was ultrasonicated for five minutes to obtain a stable ferrofluid (F). The resultant ferrofluid was divided into two portions. Rhodamine B (9.2 mg dissolved in 2.5 ml water) was added to one portion and stirred for 3 hours (FR). Silane modified ferrofluid (FG) was synthesized by the addition of a 1 ml of pre-hydrolysed GPTMS to a 20 ml of stable ferrofluid suspension (F) under constant stirring for 6 hours. The pre-hydrolysed GPTMS was obtained by adding 10 ml of water:isopropanol (1:2) mixture to 1 ml of the former under stirring for 1 hour. Further

Delivered by Publishing Technology to: Cochin University of Science and Technology
IP: 202.88.252.50 On: Fri, 05 July 2024 05:56:25
Copyright: American Scientific Publishers

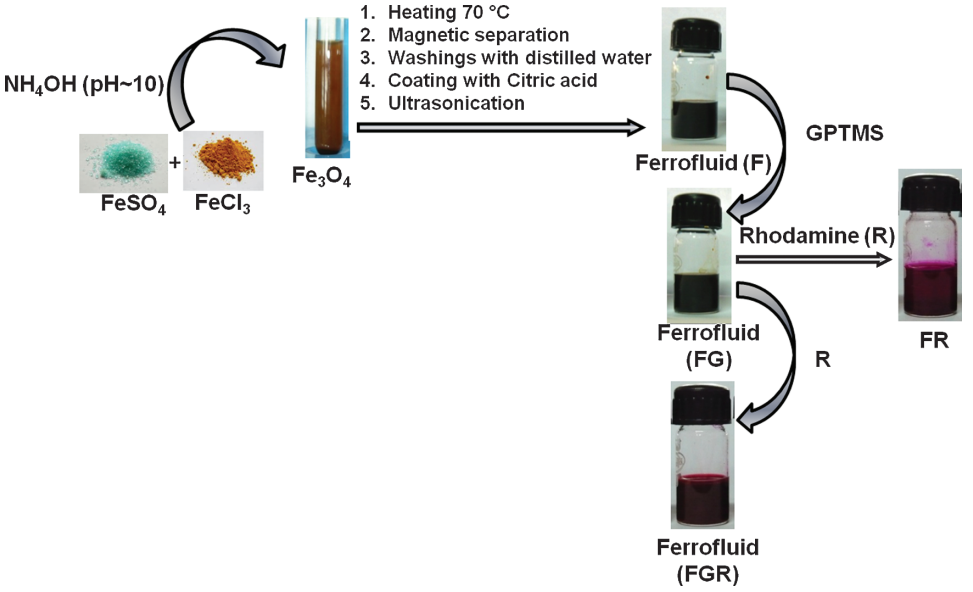

Fig. 1. Process scheme for the synthesis of ferrofluids.

rhodamine B was added to the silane modified ferrofluid under continuous stirring for 3 hours (FGR). The detailed process scheme for the synthesis of ferrofluids is provided as Figure 1. The concentration of ferrofluids estimated using gravimetric method for the samples F and FG are 7.8 mg/ml and 12 mg/ml respectively.

Copyright: American Scientific Publishers

2.3. Characterization Techniques

The ferrofluids were further characterized by various analytical techniques namely XRD (Rigaku $D_{max}C$, $\lambda = 1.5418$ Å), FT-IR (Thermo Nicolet Avatar 370 DTGS), UV spectroscopy (Hitachi U-3410 UV-Vis-NIR), photoluminescence spectroscopy (Fluoromax-3), vibrational sample magnetometry (EG&G Par 4500), zeta potential analysis (Malvern instruments MAL500909) and transmission electron microscopy (TEM, JEOL JEM 2200 FS). Fluorescence lifetime measurements were carried out in an IBH picosecond single photon counting system. The fluorescence decay profiles were deconvoluted using IBH data station software version 2.1, and fitted with a bi-exponential decay, minimizing the χ^2 values of the fit to 1 ± 0.05.

2.3.1. In Vitro MRI Imaging

All relaxation measurements were performed using a 7 T Biospec system (Bruker Biospin MRI, Billerica, MA) with a 30 cm bore, imaging gradients with an inner diameter of 60 mm, and a volume resonator with 35 mm inner diameter. Serial dilutions of the contrast agent were sealed in NMR tubes and suspended in relaxed water in order to minimize the effects of susceptibility differences between the samples and their surroundings. Spin-spin (T2) relaxation times were measured using a multi-echo spin echo sequence (TEmin = 8.5 ms, with 8.5 ms echo spacing over 24 echoes; TR = 5000 ms), and T2* relaxation times were measured using a multi-echo gradient echo sequence (TEmin = 1.92 ms, with 3.25 ms echo spacing over 16 echoes; TR = 500 ms; 30° excitation angle). All images were acquired with matching slice geometry (1 mm axial sections, 32 mm × 32 mm field-of-view over a 64 × 64 image matrix). Relaxation time constants for each sample were measured by fitting signal decay curves to a standard model in ParaVision, the operating environment for the Biospec platform.

2.3.2. In Vitro Cytotoxicity

For cytotoxicity assay, $\sim 1 \times 10^6$L-132 cells were inoculated into each well of a 96 well tissue culture plate and incubated for 12 hours at 37 °C, 5% CO_2. Cells were washed copiously with PBS, exposed to different concentrations of ferrofluid for 24 hour at 37 °C and further subjected for XTT assay following standard protocol. Briefly, ferrofluid treated cells were supplemented with 50 μl of XTT substrate (2,3-bis[2-methoxy-4-nitro-5-sulfopheny]-2H-tetrazolium-5-carboxyanilide inner salt) dissolved in buffer and kept for incubation under dark at 37 °C for 5 hour. Subsequently, the viability of the cells was measured as a function of reduction of XTT to soluble formazan by mitochondrial dehydrogenase enzyme of healthy cells. The absorbance was recorded at 480 nm using a microplate reader (Infinite M-200 Tecan). Each experiment was repeated six times, and mean and standard error were calculated.

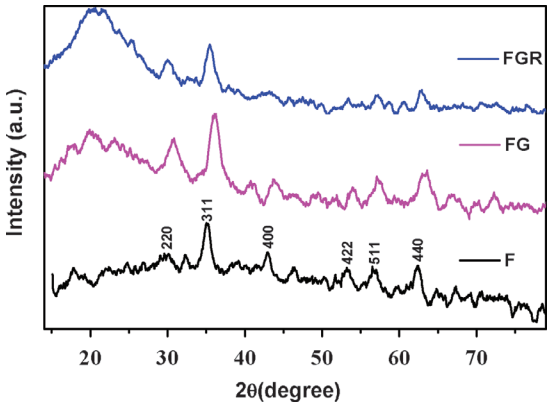

Fig. 2. XRD pattern of ferrofluids that establishes the presence of spinel structured Fe_3O_4 and amorphous silica.

3. RESULTS AND DISCUSSION

3.1. Characterization of SPIONs

XRD pattern of the ferrofluid samples is provided as Figure 2. All the diffraction peaks of ferrofluids match well with those from JCPDS data (75-0449) for iron oxide. The peaks in the graph corresponding to the crystal planes (220), (311), (400), (422), (511) and (440) established the presence of spinel structured Fe_3O_4 in the samples. In the case of FG and FGR a broad peak near 20° corresponds to amorphous silica is observed due to the functionalization with GPTMS. Crystallite size was calculated using the Debye-Scherrer equation for the strongest peak (311) and was found to be 7.6, 9.7 and 10.5 nm respectively for F, FG and FGR. Transmission electron micrographs and the particle size distribution of FG are provided in Figure 3. The particle size distribution curve shows that the average particle size of GPTMS modified iron oxide particle is 9 nm. The SAED pattern of FG given in the figure confirms the crystalline nature of the iron oxide nanoparticles. The crystal planes (311), (400), (511), (440) identified from the SAED matches well with that of XRD results and this verifies the presence of spinel structured iron oxide nanoparticles.

FTIR spectra of F, FG and FGR are given as Figure 4. The spectrum of GPTMS-modified iron oxide nanoparticles has characteristic bands of both silica and iron oxide. FG samples shows the characteristic peaks of Fe–O (673 cm^{-1}), Si–O–Si and Si–OR (a broad peak centered at 1110 cm^{-1}).[29, 30] The peaks at 942 cm^{-1} can be assigned to asymmetric stretching vibrations of the terminal groups of Si–OH. In the case of FGR the peaks due to CH_2 stretching vibrations are observed at 1466 and 2985 cm^{-1}. The presence of carboxylate groups were confirmed by the peaks at

Delivered by Publishing Technology to: Cochin University of Science and Technology

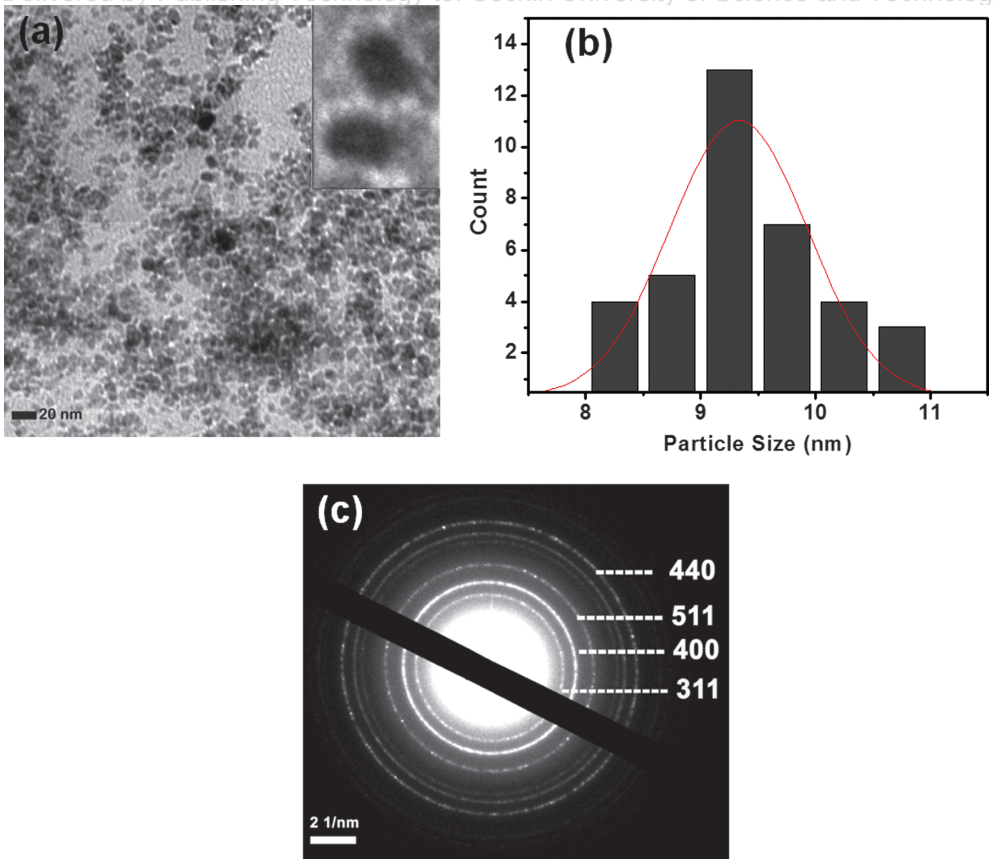

Fig. 3. (a) Transmission electron micrograph of FG (Inset: Magnified image of a single particle to show the single core single shell structure), (b) Particles size distribution, (c) SAED Pattern of FG (crystal planes identified corresponds to that of Fe_3O_4 and matches with that of XRD pattern).

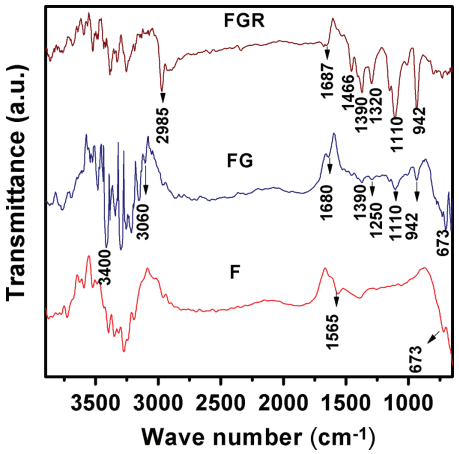

Fig. 4. FTIR spectra of F, FG and FGR showing the peaks corresponding to the presence of silica and also confirms the ring opening reactions of GPTMS.

1390 $cm^{-1}$and the characteristic C–N vibration is observed at 1327 cm^{-1}. A schematic representation of surface functionalization of SPIONS using GPTMS and rhodamine is depicted in Figure 5. It is expected that citric acid is coated over the iron oxide particles through an electrostatic attraction between the carboxylate ion and positive charge on the surface or iron oxide particles. GPTMS hydrolyses in presence of alcohol and water and the silanol group of prehydrolysed GPTMS attach to the citric acid through an ester linkage. Further upon addition of rhodamine the epoxy ring opens and link to the carboxylic acid through an esterification reaction. The ring opening is confirmed by the absence of characteristic epoxy peaks at 3060 and 1250 cm^{-1} in the FGR samples.[31]

Figure 6 provides the photographs of ferrofluids synthesized by co-precipitation technique. Photograph A in the Figure 6 illustrates the ferrofluids modified with GPTMS and rhodamine. The photographs B and C represent FGR in the presence and absence of magnetic field respectively. Photograph B was taken without a magnet and photograph C was captured after placing a button magnet below the petridish that contain FGR. The fluid accumulates at the centre of petridish in accordance with the shape of magnet placed below the petridish. Even under the influence of a magnet there was no settling or aggregation and this is a clear indication of the stability of the fluid.

3.2. ζ potential Measurements

The zeta potential values of ferrofluids were measured and are given as Table I. The zeta potential of F, FG and FGR are −38.0, −36.4 and −30.2 mV respectively which means that the ferrofluids are quite stable even after modification with GPTMS and rhodamine. However in the case of FR the zeta potential in reduced to −27.2 mV and this indicates the decrease in stability when rhodamine was incorporated into the bare ferrofluid.

Delivered by Publishing Technology to: Cochin University of Science and Technology
IP: 14.139.185.18 On: Fri, 01 Aug 2014 05:30:29
Copyright: American Scientific Publishers

3.3. Magnetization Studies

Room temperature magnetization measurements of ferrofluids were carried out and the magnetic hysteresis is given as Figure 7. The ferrofluids have negligible coercivity

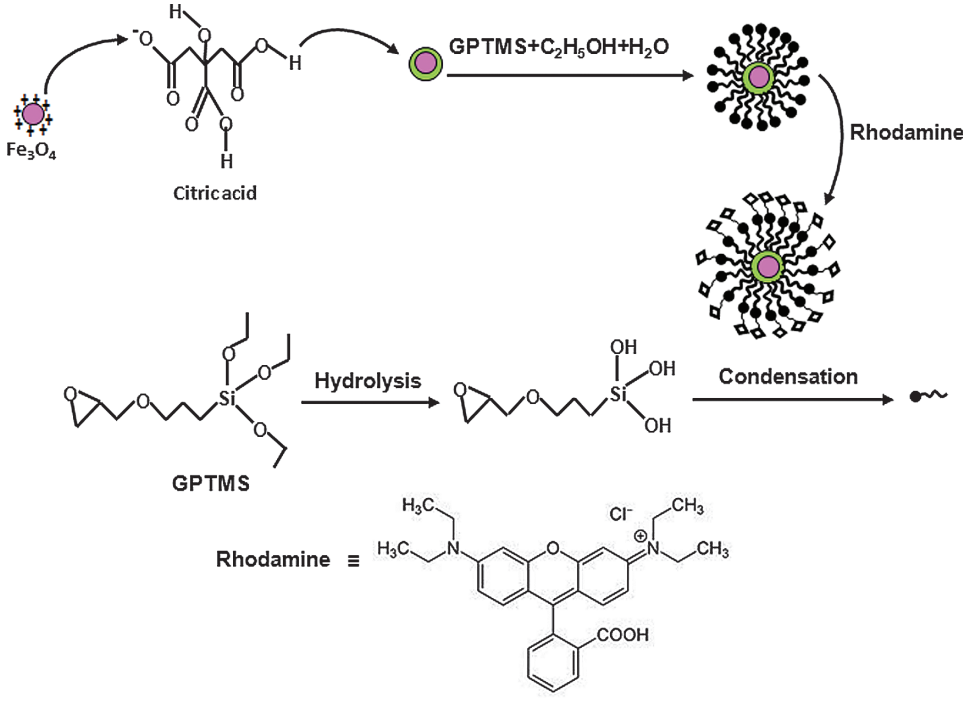

Fig. 5. Schematic illustration for the synthesis of FGR.

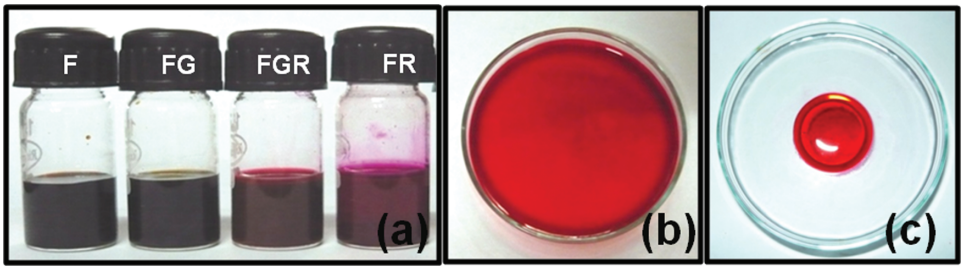

Fig. 6. Photographs of (A) Different ferrofluids, (B) FGR ferrofluid in the absence of a magnetic field, (C) FGR in the presence of a magnetic field (A round magnet is placed below the petridish).

and remanance which are the essential characteristics of superparamagnetic iron oxide nanoparticles. The saturation magnetization point of F is 65 emu/g, which upon functionalization with GPTMS (FGR) decrease to 62 emu/g. The slight decrease in magnetization occurred on modification with GPTMS and rhodamine can be attributed to the core–shell structure in which magnetic iron oxide is encircled with nonmagnetic silica and rhodamine.

3.4. UV-Visible Spectral Analysis

The UV-Visible spectra of rhodamine and ferrofluids were given as Figure 8(A). The maximum absorption of F is at 450 nm whereas it is at 446 nm for rhodamine, FR and FGR. According to the band gap calculation using a first differential analysis[32] of $h\nu$ vs $ln(\alpha h\nu)$ the band gaps of F and rhodamine are 2.08 eV and 1.97 eV respectively (given as Fig. 8(B)). When rhodamine was incorporated in to the ferrofluid the band gap was shifted from 1.97 to 1.8 eV and therefore a red shift is expected due to the influence of iron oxide nanoparticles. However the FGR has a band gap of 1.9 eV which means that the influence of iron core over the fluorescence properties was minimized due to the silica coating.

3.5. Fluorescence Studies

The emission spectra of ferrofluids obtained for an excitation wavelength 446 nm is given in Figure 9(A) and the colour coordinates (1931) for the emission of R(0.66, 0.30), FR(0.58, 0.35) and FGR (0.69, 0.30) are given as Figure 9(B). R and FGR have very close x, y coordinates which means the fluorescence property of rhodamine molecules were retained in the case of FGR. When exited at 446 nm, rhodamine shows an emission at 630 nm which is in the red region of visible spectrum. In the case of FR a very broad peak with a lower intensity is observed and it is shifted towards the higher wave number (650 nm). An inhomogeneous broadening of emission spectra towards larger wavelengths (red shift) has been reported for rhodamine in close vicinity to metallic surfaces and this was explained as an effect of the reduced excited state lifetime.[33, 34] In the present study also a red shift is observed when rhodamine was attached to iron oxide nanoparticles(FR). This can also be attributed to the reduction in excited state life time. Even though rhodamine attached to iron oxide-silica core–shell nanoparticles (FGR) also shows a red shift, the extent of shift is lower compared to FR. Cationic dyes in solution undergo a spectral shift in the presence of anions to shorter wavelengths due to the formation of cation–anion charge transfer complexes.[35, 36] Since the silica is negatively charged and the dye molecules are in proximity to the outermost negative charge, there is a strong coupling of the positively charged dye molecules with the negative charge of silica. This interaction will minimize the extent of shift towards higher wave number in the case of FGR. The photographs of ferrofluids irradiated with an excitation wavelength of 446 nm are given as Figure 10. The photographs

Delivered by Publishing Technology to: Cochin University of Science and Technology
IP: 14.139.185.18 On: Fri, 01 Aug 2014 05:50:29
Copyright: American Scientific Publishers

Table I. Zeta potential values of different ferrofluids.

Sample name	Zeta potential (mV)
F	−38.0
FG	−36.4
FR	−27.2
FGR	−30.2

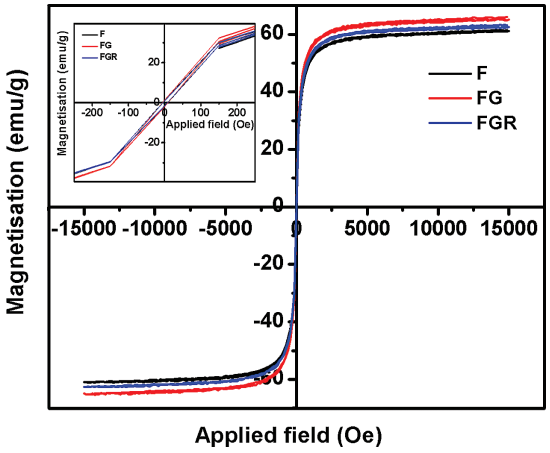

Fig. 7. Magnetic hysteresis of ferrofluids showing the superparamagnetic behaviour with a saturation magnetization of ~60 emu/g. Inset: The magnetic hysteresis plotted with a resolution of 100 Oe shows negligible coercivity and remanance.

Article

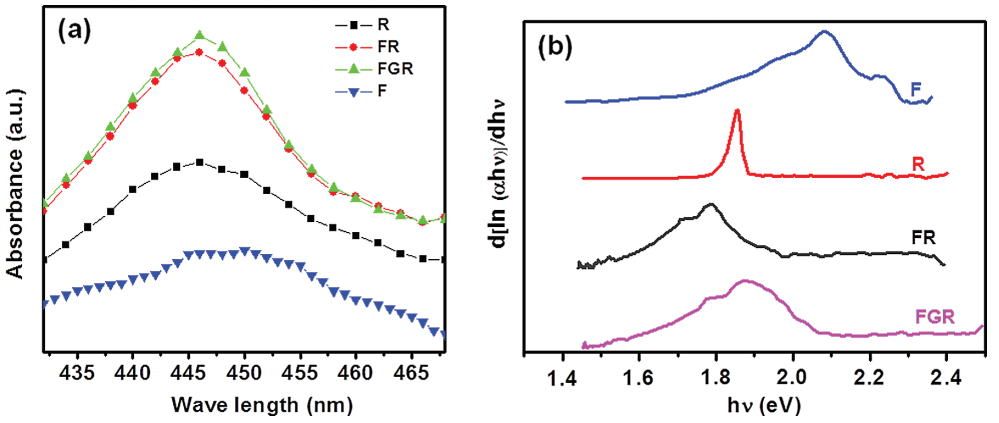

Fig. 8. (a) UV-Visible spectra of rhodamine and ferrofluids and (b) First differential analysis plot of $h\nu$ vs $ln(\alpha h\nu)$ for band gap determination.

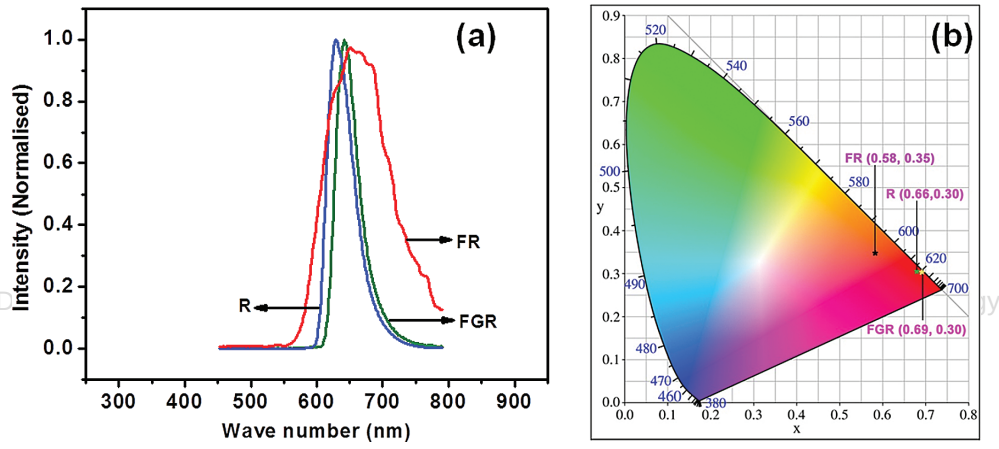

Fig. 9. (a) Emission spectra of rhodamine (R) and ferrofluids (F, FR and FGR) and (b) Chromaticity diagram showing colour coordintes for the emission of R, FR and FGR.

also illustrate that in the case of FGR the influence of iron oxide over the fluorescence of rhodamine was minimized by the intermediate coating of prehydrolysed silica particles.

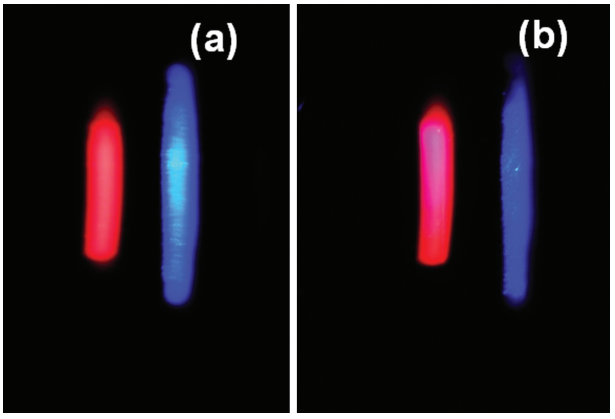

Fig. 10. Photographs of ferrofluid samples irradiated with light ($\lambda_{excitation} = 446$ nm) (a) Rhodamine and (b) FGR. Blue light corresponds to source and red is emission.

3.5.1. *Fluorescence Life Time Decay Analysis*

To further understand the luminescent process, time resolved life time decay curves of ferrofluid samples FR and FGR are given as Figure 11. The life time measurements showed a bi-exponential decay pattern when

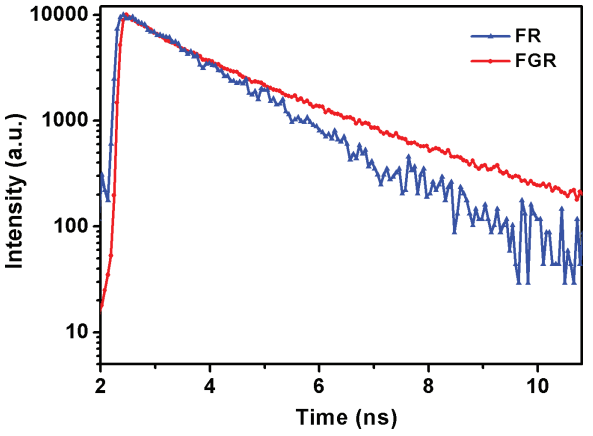

Fig. 11. Time resolved life time decay of ferrofluid samples.

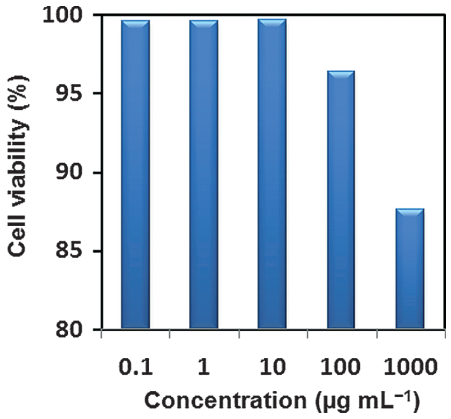

Fig. 12. XTT assay of FGR in L-132 cell showing the cell viability of the modified ferrofluids.

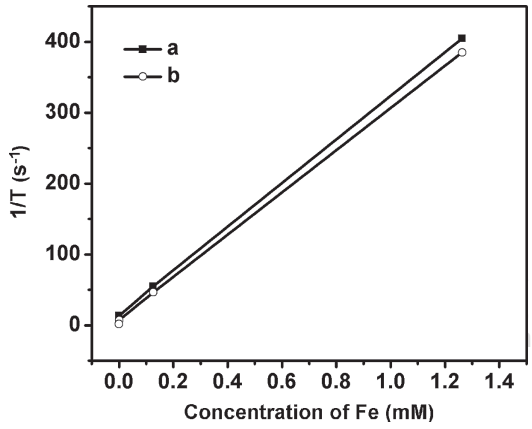

Fig. 13. Plots of inverse of relaxation time *vs* the concentration of iron in the sample (A) T2* relaxation and (B) T2 relaxation.

excited at 446 nm indicating the presence of two distinct luminescent species. In the case of FR, life time of the major component (87%) and the minor component (13%) are 1.60 ns and 0.84 ns respectively. FGR also showed a bi-exponential decay with a life time of 2.62 ns for major component (67%) and 1.13 ns for minor component (33%). The increase in life time of FGR indicates a slower decay process of the luminescent entity and therefore it can be concluded that quenching is minimum in this case.[37]

3.6. *In Vitro* Cytotoxicity

Biocompatibility and nontoxicity of nanoparticles are very much important as far as biomedical application is concerned. Figure 12 shows the viability of L-132 cells in the presence of different concentrations ferrofluid (FGR). The cell viability was measured as a function of mitochondrial dehydrogenase enzyme activity in healthy cells to reduce assay substrate XTT into water soluble formazan, measured at 480 nm. Any decrease in the release of formazan is considered as an index of mitochondrial damage and cell death. The ferrofluid did not show any decrease in the viability of human L-132 cells upto a concentration of 100 μg mL^{-1}. It may be noted that 100 μg mL^{-1} is a concentration far higher than the normal use. A marginal decrease in the viability was observed when the cells were exposed to 1000 μg mL^{-1} ferrofluid.

3.7. *In Vitro* MRI Imaging

to: Cochin University of Science and Technology
On: Fri, 01 Aug 2014 05:50:29
erican Scientific Publishers

Figure 13 provides the change in the inverse of transverse relaxation time (T2 and T2*) with respect to the concentration of iron. Slope of these plots is the relaxivity, which is a measure of the ability of a particular MRI contrast agents to increase the relaxation of the surrounding nuclear spins (hydrogen protons) and thereby improve the contrast during imaging.[38] Thus R2 and R2* relaxivity of the FGR was found out to be 334 mM^{-1}s^{-1} and 312 mM^{-1}s^{-1} respectively. The values are quite high, which is an indicative of the ability of FGR materials as negative MRI contrast agents.[39]

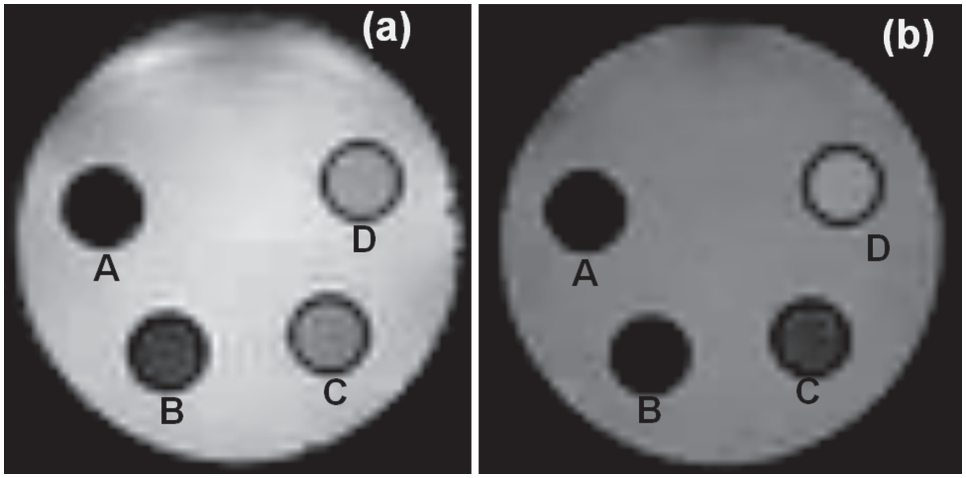

Fig. 14. (a) T2* weighted gradient echo MR phantom images of various concentration of FGR and (b) T2 weighted spin echo MR phantom images of various concentration of FGR. (A: 1.26 mM, B: 0.12 mM, C: 0.012 mM, D: Water)

Article

Figure 14 demonstrates the MR phantom images obtained from different concentrations of FGR sealed on NMR tubes and submerged on relaxed water. From the image, it can be observed that the contrast shown by FGR dilutions is greater in comparison to relaxed water. Even with a 0.012 mM of FGR good contrast is obtained indicating its potential as a MRI contrast agent.

4. CONCLUSION

A multimodal fluorescent nano probe based on SPIONS with a high saturation magnetization of ~62 emu/g and a visible luminescent emission of 640 nm ($\lambda_{excitation}$ = 446 nm) was developed using rhodamine as the fluorescent entity. The core–shell structure was designed in such a way that fluorescence quenching by the inner magnetic core was minmized by means of an intermediate passive layer of silica that was developed over the iron oxide particles by a prehydrolyzed GPTMS. The increase in life time in the case of FGR observed in the time resolved measurements indicates a slower decay process of the luminescent entity and therefore it is assumed that quenching is minimum in this case. Structural investigations by FTIR back up the possibility of functionalisation of hydrolyzed GPTMS over the SPIONs through an ester linkage and further epoxy ring opening of GPTMS through which attachment to the rhodamine molecules take place. The *in vitro* studies on human L-132 embryonic lung cells revealed that these materials can find potential application especially in biomedical fields in the simultaneous diagnosis and treatment of diseases like cancer. The *in vitro* MR imaging demonstrated a high contrast when these multimodal nano probe was employed and the R2 relaxivity of these sample was found to be 334 $mM^{-1}s^{-1}$ which reveals its high potential as a T2 contrast enhancing agent.

Acknowledgments: The author Sasidharan Smitha acknowledges University Grants Commission (UGC, India) for the financial assistance in the form of D S Kothari postdoctoral fellowship (No. F.4-2/2006 (BSR) 13-247/2008) and Department of Science and Technology (DST, India) for the fast track project (SERB/F/1823/2012-13). We would also like to acknowledge Dr. Mahesh Hariharan, IISER, Thiruvananthapuram for the life time decay measurements and MD Anderson Cancer Center, USA for the small animal facility MRI (funded by the Cancer Center Support Grant from the National Cancer Institute (CA016672)).

References and Notes

1. H. Lu, E. L. Salabas, and F. Schuth; Magnetic nanoparticles: synthesis, protection, functionalization, and application; *Angew. Chem. Int. Ed.* 46, 1222 **(2007)**.
2. Q. A. Pankhurst, J. Connolly, S. K. Jones, and J. Dobson; Applications of magnetic particles in biomedicine; *J. Phys. D: Appl. Phys.* 36, 167 **(2003)**.
3. V. Omid, J. W. Gunn, and M. Zhang; Design and fabrication of magnetic nanoparticles for targeted drug delivery and imaging; *Adv. Drug Deliv. Rev.* 62, 284 **(2010)**.
4. T. N. Narayanan, B. K. Gupta, S. A. Vithayathil, R. R. Aberto, S. A. Mani, J. T.-Tijerina, B. Xie, B. A. Kaipparettu, S. V. Torti, and P. M. Ajaya; Hybrid 2D nanomaterials as dual-mode contrast agents in cellular imaging; *Adv. Mater.* 24, 2992 **(2012)**.
5. A. C. Poulose, S. Veeranarayanan, A. Aravind, Y. Nagaoka, Y. Yoshida, T. Maekawa, and D. Sakthi Kumar; Synthesis of $CuAlS_2$ nanocrystals and their application in bio-imaging *Mater. Express* 2, 94 **(2012)**.
6. S. K. Sonkar, M. Ghosh, M. Roy, A. Begum, and S. Sarkar; Carbon nano-onions as nontoxic and high-fluorescence bioimaging agent in food chain—An *in vivo* study from unicellular *E. coli* to multicellular *C. Elegans*; *Mater. Express* 2, 105 **(2012)**.
7. H. M. Kim, H. Lee, K. S. Hong, M. Y. Cho, M. H. Sung, H. Poo, and Y. T. Lim; Synthesis and high performance of magnetofluorescent polyelectrolyte nanocomposites as MR/Near-infrared multimodal cellular imaging nanoprobes; *ACS Nano* 5, 8230 **(2011)**.
8. J. A. Barreto, W. O'Malley, M. Kubeil, B. Graham, H. Stephan, and L. Spiccia; Nanomaterials: applications in cancer imaging and therapy; *Adv. Mater.* 23, H18 **(2011)**.
9. J. E. Lee, N. Lee, H. Kim, J. Kim, S. H. Choi, J. H. Kim, T. Kim, I. C. Song, S. P. Park, W. K. Moon, and T. Hyeon; Uniform mesoporous dye-doped silica nanocrystals for simultaneous enhanced magnetic resonance imaging, fluorescence imaging, and drug delivery; *J. Am. Chem. Soc.* 132, 552 **(2010)**.
10. N. Chekina, D. Horák, P. Jendelová, M. Trchová, M. J. Beneš, M. Hrubý, V. Herynek, K. Turnovcová, and E. Syková; Fluorescent magnetic nanoparticles for biomedical applications; *J. Mater. Chem.* 21, 7630 **(2011)**.
11. J. Xie, G. Liu, H. S. Eden, H. Ai, and X. Chen; Surface-engineered magnetic nanoparticle platforms for cancer imaging and therapy; *Acc. Chem. Res.* 44, 883 **(2011)**.
12. S. A. Corr, Y. P. Rakovich, and Y. K. Gun'ko; Multifunctional magnetic-fluorescent nanocomposites for biomedical applications; *Nanoscale Res. Lett.* 3, 87 **(2008)**.
13. F. Erogbogbo, K. T. Yong, R. Hu, W. C. Law, H. Ding, C. W. Chang, P. N. Prasad, and M. T. Swihart; Biocompatible magnetofluorescent probes: luminescent silicon quantum dots coupled with superparamagnetic iron (III) oxide; *ACS Nano* 4, 5131 **(2010)**.
14. Z. Ali, A. Z. Abbasi, F. Zhang, P. Arosio, A. Lascialfari, M. F. Casula, A. Wenk, W. Kreyling, R. Plapper, M. Seidel, R. Niessner, J. Knöll, A. Seubert, and W. J. Parak; Multifunctional nanoparticles for dual imaging; *Anal. Chem.* 83, 2877 **(2011)**.
15. T. Neuberger, B. Schöpf, H. Hofmann, M. Hofmann, and B. V. Rechenberg; Superparamagnetic nanoparticles for biomedical applications: possibilities and limitations of a new drug delivery system; *J. Magn. Magn. Mater.* 293, 483 **(2005)**.
16. C. C. Huang, C. Y. Tsai, H. S. Sheu, K. Y. Chuang, C. H. Su, U. S. Jeng, F. Y. Cheng, C. H. Su, H. Y. Lei, and C. S. Yeh; Enhancing transversal relaxation for magnetite nanoparticles in MR imaging using Gd^{3+}-chelated mesoporous silica shells; *ACS Nano* 5, 3905 **(2011)**.
17. Y. Zhang, G. K. Das, R. Xu, and T. T. Y. Tan; Tb-doped iron oxide; bifunctional fluorescent and magneticnanocrystals; *J. Mater. Chem.* 19, 3696 **(2009)**.
18. J. J. Gallagher, R. Tekoriute, J. Ann O'Reilly, C. Kerskens, Y. K. Gun'ko, and M. Lynch; Bimodal magnetic-fluorescent nanostructures for biomedical applications; *J. Mater. Chem.* 19, 4081 **(2009)**.
19. Y. Lu, Y. Yin, B. T. Mayers, and Y. Xia; Modifying the surface properties of superparamagnetic iron oxide nanoparticles through a sol–gel approach; *Nano Lett.* 2, 183 **(2002)**.
20. R. Kumar, I. Roy, T. Y. Ohulchanskyy, L. N. Goswami, A. C. Bonoiu, E. J. Bergey, K. M. Tramposch, A. Maitra, and

Delivered by Publishing Technology to: Cochin University of Science and Technology
IP: 14.139.125.99 On: Fri, 04 Apr 2014 05:15:58
Copyright: American Scientific Publishers

P. N. Prasad; Covalently dye-linked, surface-controlled, and bioconjugated organically modified silica nanoparticles as targeted probes for optical imaging; *ACS Nano* 2, 449 **(2008)**.

21. P. Y. Kang, L. C. Wei, H. Y. Hsuan, T. K. Chun, and C. P. Tai; Multifunctional mesoporous silica-coated hollow manganese oxide nanoparticles for targeted optical imaging, T_1 magnetic resonance imaging and photodynamic therapy; *Mater. Express* 1, 136 **(2011)**.

22. S. W. Ha, C. E. Camalier, G. R. Beck, and J. K. Lee; New method to prepare very stable and biocompatible fluorescentsilica nanoparticles; *Chem. Commun.* 20, 2881 **(2009)**.

23. Y. K. Peng, C. W. Lai, Y. H. Hsiao, K. C. Tang, and P. T. Chou; Multifunctional mesoporous silica-coated hollow manganese oxide nanoparticles for targeted optical imaging, T_1 magnetic resonance imaging and photodynamic therapy; *Mater. Express* 1, 136 **(2011)**.

24. P. Shajesh, S. Smitha, P. R. Aravind, and K. G. K. Warrier; Synthesis, structure and properties of cross-linked $R(SiO_{1.5})/SiO_2$ (R = 3-glycidoxypropyl) porous organic inorganic hybrid networks dried at ambient pressure; *J. Colloid Interface Sci.* 336, 691 **(2009)**.

25. T. Ninjbadgar, and D. F. Brougham; Epoxy ring opening phase transfer as a general route to water dispersible superparamagnetic Fe_3O_4 nanoparticles and their application as positive MRI contrast agents; *Adv. Funct. Mater.* 21, 4769 **(2011)**.

26. N. Tran and T. J. Webster; Magnetic nanoparticles: biomedical applications and challenges; *J. Mater. Chem.* 20, 8760 **(2010)**.

27. S. K. Mandal, N. Lequeux, B. Rotenberg, M. Tramier, J. Fattaccioli, J. Bibette, and B. Dubertret; Encapsulation of magnetic and fluorescent nanoparticles in emulsion droplets; *Langmuir* 21, 4175 **(2005)**.

28. R. G. Aswathy, B. Sivakumar, D. Brahatheeshwaran, T. Ukai, Y. Yoshida, T. Maekawa, and D. Sakthi Kumar; Biocompatible fluorescent jelly quantum dots for bioimaging; *Mater. Express* 1, 291 **(2011)**.

29. A. P. Reena Mary, T. N. Narayanan, V. Sunny, D. Sakthikumar, Y. Yasuhiko, P. A. Joy, and M. R. Anantharaman; Synthesis of bio-compatible SPION-based aqueous ferrofluids and evaluation of radio frequency power loss for magnetic hyperthermia; *Nanoscale Res. Lett.* 5, 1706 **(2010)**.

30. T. N. Narayanan, A. P. Reena Mary, P. K. Anas Swalih, D. Sakthi Kumar, D. Makarov, M. Albrecht, J. Puthumana, A. Anas, and M. R. Anantharaman; Enhanced bio-compatibility of ferrofluids of self-assembled superparamagnetic iron oxide-silica core–shell nanoparticles; *J. Nanosci. Nanotechnol.* 11, 1958 **(2011)**.

31. M. C. Gutiérrez, M. J. Hortigüela, M. L. Ferrer, and F. D. Monte; Highly fluorescent rhodamine b nanoparticles entrapped in hybrid glasses; *Langmuir* 23, 2175 **(2007)**.

32. S. Chakrabarti, D. Ganguli, and S. Chaudhuri; Optical properties of γ-Fe_2O_3 nanoparticles dispersed on sol–gel silica spheres; *Physica E* 24, 333 **(2004)**.

33. G. Cnossen, K. E. Drabe, and D. A. Wiersma; Fluorescence properties of sub monolayers of rhodamine 6G in front of a mirror; *J. Chem. Phys.* 98, 5276 **(1993)**.

34. T. Baumgartel, C. V. Borczyskowski, and H. Graaf; Fluorescence studies of Rhodamine 6G functionalized silicon oxide nanostructures; *Nanotechnology* 21, 475205 **(2010)**.

35. M. Schubert and D. Hamerman; Metachromasia; Chemical theory and histochemical use; *J. Histochem. Cytochem.* 4, 159 **(1956)**.

36. M. K. Pal and S. K. Ash; Metachromasia of basic dyes induced by mercuric chloride II; *J. Phys. Chem.* 78, 536 **(1973)**.

37. K. Itoh, Y. Chiyokawa, M. Nakao, and K. Honda; Fluorescence quenching processes of Rhodamine B on oxide semiconductors and light-harvesting action of its dimers; *J. Am. Chem. Soc.* 106, 1620 **(1984)**.

38. T. Ahmad, H. Bae, I. Rhee, Y. Chang, J. Lee, and S. Hong; Particle size dependence of relaxivity for silica-coated iron oxide nanoparticles; *Curr. Appl. Phys.* 12, 969 **(2012)**.

39. N. Lee and T. Hyeon; Designed synthesis of uniformly sized iron oxide nanoparticles for efficient magnetic resonance imaging contrast agents; *Chem. Soc. Rev.* 41, 2575 **(2012)**.

Delivered by Publishing Technology to: Cochin University of Science and Technology
IP: 202.88.252.51 On: Fri, 04 Apr 2014 05:45:39
Copyright: American Scientific Publishers

Received: 6 August 2012. Revised/Accepted: 12 October 2012.